Flagellar perturbations activate adhesion through two distinct pathways in *Caulobacter crescentus*

David M. Hershey[2], Aretha Fiebig[1] and Sean Crosson[1] #

[1] Department of Microbiology and Molecular Genetics, Michigan State University, East Lansing, MI 48824, USA

[2] Department of Biochemistry and Molecular Biology, University of Chicago, Chicago, IL 60637, USA

Running title: Flagellar signaling in *C. crescentus*

To whom correspondence should be addressed: crosson4@msu.edu; (517) 884-5345

Keywords: Adhesion, flagellum, motility, holdfast, biofilm

Abstract: Bacteria carry out sophisticated developmental programs to colonize exogenous surfaces. The rotary flagellum, a dynamic machine that drives motility, is a key regulator of surface colonization. The specific signals recognized by flagella and the pathways by which those signals are transduced to coordinate adhesion remain subjects of debate. Mutations that disrupt flagellar assembly in the dimorphic bacterium *Caulobacter crescentus* stimulate the production of a polysaccharide adhesin called the holdfast. Using a genome-wide phenotyping approach, we compared surface adhesion profiles in wild-type and flagellar mutant backgrounds of *C. crescentus*. We identified a diverse set of flagellar mutations that enhance adhesion by inducing a hyper-holdfast phenotype and discovered a second set of mutations that suppress this phenotype. Epistasis analysis of the *flagellar signaling suppressor* (*fss*) mutations demonstrated that the flagellum stimulates holdfast production via two genetically distinct pathways. The developmental regulator PleD contributes to holdfast induction in mutants disrupted at both early and late stages of flagellar assembly. Mutants disrupted at late stages of flagellar assembly, which retain an intact rotor complex, induce holdfast production through an additional process that requires the MotAB stator and its associated diguanylate cyclase, DgcB. We have assigned a subset of the *fss* genes to either the stator- or *pleD*-dependent networks and characterized two previously unidentified motility genes that contribute to the stator-dependent pathway. We propose a model in which the flagellum integrates both developmental and mechanical stimuli to coordinate adhesion.

Importance: Understanding how bacteria colonize solid surfaces is of significant clinical, industrial and ecological importance. In this study, we identified genes that are required for *Caulobacter crescentus* to activate surface attachment in response to signals from a macromolecular machine called the flagellum. Genes involved in transmitting information from the flagellum can be grouped into separate pathways, those that control the *C. crescentus* developmental program and those that

are required for flagellar rotation. Our results support a model in which a developmental and a mechanical signaling pathway operate in parallel downstream of the flagellum and converge to regulate adhesion. We conclude that the flagellum serves as a signaling hub by integrating internal and external cues to coordinate surface colonization and emphasize the role of signal integration in linking complex sets of environmental stimuli to individual behaviors.

Introduction: For microorganisms, solid surfaces serve as sites of nutrient accumulation, gateways into host tissues and shelters from environmental stresses (1–3). To access surface-associated niches, bacteria deploy specialized programs for seeking, recognizing and colonizing objects in their surroundings (4). These programs culminate in a pronounced transition away from a free-living, exploratory state and toward an adherent, sessile lifestyle (5–7). Sophisticated signaling networks that integrate a host of environmental cues are used to coordinate the motile-to-sessile switch (8–10). The complexity of these circuits reflects the perilous nature of committing to colonization programs under sub-optimal conditions.

A transenvelope machine called the flagellum drives cellular motility and plays a critical role at numerous stages of surface colonization(11, 12). The flagellum is synthesized in a stepwise process that is controlled by a transcriptional hierarchy(13). Assembly begins with the expression of class II genes that code for a rotor and secretion subcomplex that are inserted in the cytoplasmic membrane(14, 15). Upon completion of the class II program, assembly proceeds outward with the incorporation of an envelope spanning basal body (class III genes) followed by the secretion of an extracellular filament (class IV genes) (16, 17). Stator subcomplexes that surround the rotor utilize ion gradients across the cytoplasmic membrane to generate torque by turning the hook-basal body complex and its associated filament, propelling the cell forward (Fig 1B)(18, 19). Flagellar motors are highly attuned to environmental conditions. They support motility under diverse conditions,

63 modulate torque in response to changing loads and alter rotational bias to support complex
64 swimming patterns(20–23).

65 Paradoxically, flagellar motility must be repressed during sessile growth but is also required
66 for efficient surface colonization(6, 24–26). During the initial stages of attachment, swimming is
67 thought to promote productive interactions with target substrates by providing energy needed to
68 overcome repulsive forces at the liquid-solid interface(27). The flagellum is also thought to play an
69 additional regulatory role in activating the motile-to-sessile transition by recognizing physical
70 contact with solid substrates(11). Such tactile sensing events serve as critical cues for initiating
71 colonization programs, but the mechanistic basis for how bacteria sense and respond to physical
72 stimuli remains controversial.

73 The dimorphic bacterium *Caulobacter crescentus* is uniquely adapted to surface colonization.
74 Cell division in *C. crescentus* is asymmetric and yields to two distinct cell types(28). Newborn
75 swarmer cells are flagellated, produce type IV pili (T4P) and cannot initiate replication (29, 30).
76 These motile cells undergo a morphogenic transition to become replication-competent stalked cells
77 by replacing their flagellum and pili with a specialized envelope extension called the stalk(31).
78 During the swarmer-to-stalked transition, *C. crescentus* can produce a polysaccharide adhesin called
79 the holdfast that is displayed at the tip of the stalked cell where it promotes attachment to surfaces
80 (Fig 1A) (7, 32). Holdfast production is the primary determinant of surface colonization in *C.*
81 *crescentus,* and its regulation is elaborate (26, 33). In addition to cell cycle cues(7, 34), nutrient
82 availability(35), light(36) and redox status(37), mechanical contact has been implicated as an
83 important activator of holdfast assembly (38). Recent evidence suggests that both flagella and T4P
84 can stimulate holdfast production in response to contact with a surface(39, 40), but conflicting
85 models have emerged for how these transenvelope machines survey and disseminate mechanical
86 information(34, 41).

87 Here, we used an unbiased phenotyping approach called adhesion profiling to show that a
88 diverse set of flagellar mutations induce a hyper-holdfast phenotype in *C. crescentus* and to identify
89 dozens of *flagellar signaling suppressor* (*fss*) genes that contribute to holdfast stimulation
90 downstream of the flagellum. *fss* mutations suppress the hyper-adhesive effects of flagellar
91 disruption through two distinct pathways. Select regulators of cell-cycle progression are involved
92 in stimulating adhesion upon flagellar disruption, while components of the stator subcomplexes
93 contribute to holdfast stimulation specifically in mutants that can assemble an inner membrane
94 rotor. We assigned two previously uncharacterized genes roles in the stator-dependent pathway
95 and demonstrated that they contribute to force generation by the flagellar motor by promoting
96 robust swimming. Our results indicate that the flagellum serves as a signaling hub by integrating
97 mechanical and developmental cues to coordinate surface colonization programs.
98
99 **Results:**
100 *A complex gene network links the flagellum to holdfast production*
101 We previously described a method called adhesion profiling by which a barcoded transposon
102 library is sequentially passaged in the presence of a cellulose-based substrate. Adhesive mutants
103 become depleted as they colonize the substrate, enriching for mutants with attachment defects in
104 the surrounding broth. By monitoring the mutant population over time, we quantified each gene's
105 contribution to adhesion at the genome scale (33). This initial study identified a set of hyper-
106 adhesive mutants that included genes involved in flagellar assembly, which suggested that certain
107 genetic perturbations to the flagellum stimulate holdfast production by mimicking surface contact
108 (Fig 1C). We modified our genetic selection to identify a broader range of adhesion-activating
109 mutations by using a defined medium in which holdfast production is almost entirely repressed in
110 wild-type *C. crescentus*(35). Under these conditions, dozens of genes displayed adhesion profiles

111 indicative of hyper-adhesion (Fig 1D and Table S1). Though numerous functional categories were
112 represented in this gene set, the overwhelming majority of hyper-adhesive phenotypes were
113 observed in mutants with predicted disruptions to flagellar assembly, chemotaxis or other flagellar
114 processes.

115 The gain-of-function phenotypes identified in flagellar mutants provided an attractive
116 opportunity to dissect the link between the flagellum and adhesion. A mutant (Δ*flgH*) lacking the
117 gene for the flagellar L ring protein(42) displayed a hyper-holdfast phenotype under our selection
118 conditions(34)(Fig 1C). We therefore constructed a barcoded Tn-*Himar1* library in a Δ*flgH*
119 background and performed a second adhesion profiling experiment in order to identify mutations
120 that suppress the hyper-holdfast phenotype. As in wild type, genes required for holdfast synthesis
121 (*hfs*) were the strongest determinants of adhesion in the Δ*flgH* mutant. However, we also identified
122 a few dozen genes (called *fss* for flagellar signaling suppressor) that contribute to adhesion
123 specifically in the Δ*flgH* background (Fig 1E, Table S2). While, many of the *fss* genes are
124 uncharacterized, insertions in genes known to participate in flagellar rotation, chemotaxis, cell cycle
125 control and other physiological processes had *fss* phenotypes as well. Both the abundance and
126 functional diversity of the suppressors point to a complex signaling network that links adhesion to
127 flagellar motility.

128

129 *Distinct adhesion patterns in flagellar assembly mutants*

130 Two of the *fss* genes, *motB* and *pleD*, are known to regulate holdfast production under specific
131 conditions. *motB,* which codes for one of the flagellar stator proteins, is required for rapid holdfast
132 synthesis after surface contact in microfluidic chambers(40). *pleD,* which codes for a diguanylate
133 cyclase that regulates morphogenesis during the swarmer-to-stalked transition(43), contributes to
134 increased holdfast production in a flagellar hook mutant background through a process

135 independent of surface contact(34). These previous studies have led to conflicting models for how
136 surface contact, flagellar assembly and filament rotation modulate holdfast production. Identifying
137 mutations in both *pleD* and *motB* as suppressors of Δ*flgH* suggested that we could clarify the
138 signaling pathway that links flagellar perturbations to holdfast production.

139 We measured crystal violet (CV) staining of surface attached cells to examine how disrupting
140 *pleD* and *motB* affects adhesion to polystyrene in various flagellar mutant backgrounds. Disrupting
141 the early stages of flagellar assembly by deleting the class II genes *fliF* or *fliM* led to a hyper-adhesive
142 phenotype that was strongly suppressed by deletion of *pleD* but that was not affected by deletion of
143 *motB.* In contrast, when holdfast production was stimulated by deletion of the class III gene *flgH* or
144 disruption of flagellin secretion (Δ*flmA*)(44), the hyper-adhesive phenotype was suppressed by
145 introducing either a *pleD* or a *motB* deletion (Fig 2A). Thus, flagellar mutants stimulate adhesion
146 through different mechanisms. Mutants that disrupt the early stages of assembly activate holdfast
147 production through *pleD*, while mutants in which assembly is stalled at later stages stimulate
148 adhesion through both *pleD* and *motB.*

149

150 *Two pathways modulate holdfast production downstream of the flagellum*

151 The distinct suppression patterns in *pleD* and *motB* mutants indicated that multiple pathways
152 function downstream of the flagellum to influence adhesion. Indeed, combining the Δ*pleD* and
153 Δ*motB* mutations reduced CV staining to near un-detectable levels in both the wild-type and Δ*flgH*
154 backgrounds, supporting the model that *pleD* and *motB* control attachment through distinct
155 mechanisms (Fig 2B). The severe adhesion defect observed in cultures of the Δ*pleD* Δ*motB* double
156 mutant demonstrates that the *pleD*- and *motB*-dependent pathways do not operate exclusively in
157 the context of flagellar mutants. Either the *pleD* or *motB* pathway must be intact for *C. crescentus* to
158 colonize surfaces.

159 We quantified holdfast production by staining cells from a representative panel of mutants
160 with fluorescently-labelled wheat germ agglutinin (fWGA). The proportion of cells displaying a
161 holdfast was elevated in both early (Δ*fliF*) and late (Δ*flgH*) flagellar assembly mutants, and the
162 suppression patterns seen by CV staining were recapitulated with fWGA staining. Holdfast
163 production was elevated to similar levels in Δ*fliF* and Δ*fliF* Δ*motB* but nearly eliminated in Δ*fliF*
164 Δ*pleD.* Introducing either the Δ*pleD* or the Δ*motB* mutations reduced holdfast production in a Δ*flgH*
165 background, and holdfast production was nearly undetectable in Δ*pleD* Δ*motB* and Δ*flgH* Δ*pleD*
166 Δ*motB* cultures (Fig 2C and Table S3). We did identify modest discrepancies between the holdfast
167 production and polystyrene colonization measurements. Although surface attachment was
168 indistinguishable from wild type in Δ*motB* cultures, holdfast production in this mutant was
169 elevated. This agrees with our previous finding that non-motile strains display holdfast-
170 independent surface colonization defects(33). Separately, CV staining was higher in Δ*flgH* cultures
171 than in Δ*fliF* cultures, but the proportion of holdfast producing cells was higher in the Δ*fliF* mutant.
172 Because both strains are non-motile, the discrepancy is likely due to modulation of additional
173 holdfast-independent colonization factors such as type IV pilus dynamics(33, 45).

174 Finally, we examined expression of the *holdfast inhibitor A* (*hfiA*) gene, a key regulator that
175 inhibits adhesion by targeting a glycosyltransferase in the holdfast biosynthesis pathway (Fig
176 2D)(35). Expression of *hfiA* is finely tuned by a complex hierarchy of transcription factors such that
177 small changes in expression have significant impacts on holdfast production (33, 35, 37). Increased
178 holdfast production in the Δ*flgH* and Δ*motB* backgrounds is accompanied by a decrease in P_{hifA}-*lacZ*
179 reporter activity, but holdfast production is stimulated in the Δ*fliF* mutant without a reduction in
180 *hfiA* transcription (Fig 2D and Table S3). Introducing either the Δ*motB* or Δ*pleD* mutations into the
181 Δ*flgH* background restored P_{hifA} expression to wild-type levels. These measurements show that *pleD*
182 is required for downregulation of *hfiA* in the Δ*flgH* background, but do not clarify the role of *motB.*

183 It remains unclear how the Δ*motB* mutation reduces *hfiA* promoter activity in the wild-type
184 background but rescues the reduced expression in a Δ*flgH* mutant. Finally, transcription from the
185 *hfiA* promoter was elevated in the Δ*pleD* Δ*motB,* the Δ*flgH* Δ*pleD* Δ*motB* and the Δ*fliF* Δ*pleD* mutants,
186 indicating that activation of *hfiA* expression contributes to the severe holdfast production defect in
187 these three strains.
188
189 *Parsing regulatory networks with epistasis analysis*
190 The distinct activation profiles observed in early and late flagellar assembly mutants were used to
191 assign *fss* genes to either the *pleD*- or *motB*-dependent signaling pathways. We predicted that *pleD*
192 and other genes involved in morphogenesis make up a "developmental" signaling pathway and that
193 genes associated with signaling through the stators make up a second, "mechanical" pathway. This
194 model predicts that developmental pathway mutants should block holdfast stimulation in both
195 early and late flagellar assembly mutant backgrounds, while mechanical pathway mutants should
196 suppress hyper-adhesion specifically in late assembly mutants. Two additional *fss* genes, *shkA* and
197 *dgcB,* were used to test these predictions. *shkA* encodes a histidine kinase that regulates stalk
198 development(46), and *dgcB* codes for a diguanylate cyclase that physically associates with stator
199 subcomplexes(40). Deleting *shkA* suppressed the hyper-adhesive effects of both the Δ*fliF* (early)
200 and the Δ*flgH* (late) mutations, while deleting *dgcB* suppressed adhesion in the Δ*flgH* background
201 but had no effect in the Δ*fliF* background (Fig 3A). These results provide further support for a model
202 in which both a developmental pathway associated with stalked cell morphogenesis and a
203 mechanical pathway associated with stator activity function downstream of the flagellum to
204 activate adhesion.
205 We also used epistasis to place two uncharacterized genes identified as Δ*flgH* suppressors
206 into the mechanical signaling pathway. *fssA* (*CC_1064*; *CCNA_01117*) encodes a protein with a

207 Sec/SP1 secretion signal and no predicted functional domains. *fssB* (*CC_2058*; *CCNA_02137*) encodes
208 a protein with a Sec/SP1 secretion signal and a predicted tetratricopeptide repeat (TPR) domain.
209 Deleting either *fssA* or *fssB* had little effect on adhesion in the wild-type or Δ*fliF* backgrounds but
210 suppressed the hyper-adhesive phenotype in Δ*flgH* (Fig 3A), demonstrating that *fssA* and *fssB*
211 contribute to holdfast stimulation through the stator-dependent, mechanical pathway.
212
213 *New motility factors contribute to mechanical activation*
214 To understand how *fssA* and *fssB* contribute to mechanical activation of holdfast synthesis, we
215 examined the motility phenotypes of the Δ*fssA* and Δ*fssB* deletions. Both mutants were severely
216 impaired in their ability to spread through soft agar. We then examined flagellar filament assembly
217 by introducing a flagellin allele ($fljK^{T103C}$) that codes for an FljK protein with a cysteine residue that
218 can be stained with maleimide-conjugated dyes(34). Flagellar filaments were evident in Δ*fssA* and
219 Δ*fssB*, indicating that the soft-agar motility defects in these mutants do not result from disruptions
220 to flagellar assembly. Examination of individual cells in liquid broth revealed that Δ*fssB* cells were
221 non-motile, while Δ*fssA* cells retained the ability to swim (Fig 3C). Thus, the Δ*fssB* mutant displays
222 a paralyzed flagellum phenotype analogous to a Δ*motB* mutant, but the motility defect of Δ*fssA* is
223 specific to soft agar, which is predicted to exert higher load on the flagellum. We conclude that *fssA*
224 and *fssB* affect the ability of the flagellar motor to drive filament rotation.
225
226 *Separate mechanisms for activating c-di-GMP production*
227 Despite the fact that the developmental and mechanical pathways can be separated genetically, they
228 ultimately converge to modulate holdfast production. Each pathway includes a diguanylate cyclase
229 predicted to synthesize bis-(3'-5')-cyclic diguanosine monophosphate (c-di-GMP), a second
230 messenger that promotes surface-associated behaviors in bacteria(47). In *C. crescentus,* c-di-GMP

231 binds numerous downstream effectors to activate stalk assembly(48), cell cycle progression(49, 50)
232 and holdfast synthesis (40, 51). To test the role of c-di-GMP synthesis in linking cues from the
233 flagellum to holdfast production, we examined catalytically inactive alleles of *pleD* and *dgcB.* In
234 contrast to wild-type alleles, $pleD^{E370Q}$(52) and $dgcB^{E261Q}$(40) failed to restore hyper-adhesion in the
235 Δ*flgH* Δ*pleD* and Δ*flgH* Δ*dgcB* backgrounds, respectively, confirming that c-di-GMP synthesis is
236 required to support flagellar signaling through both the mechanical and developmental pathways
237 (Fig 4A).

238 We further examined mechanisms by which the diguanylate cyclase activities of PleD and
239 DgcB are activated during flagellar signaling. PleD contains a receiver domain at its N-terminus that
240 includes a canonical aspartyl phosphorylation site(52, 53). Introducing the non-phosphrylatable
241 $pleD^{D53N}$ allele failed to restore hyper-adhesion in the Δ*flgH* Δ*pleD* background. We conclude that
242 phosphorylation of the PleD receiver domain is required for flagellar perturbations to stimulate
243 holdfast production through the developmental pathway (Fig 4A). Proton translocation by MotAB
244 stators is used to generate torque for flagellar filament rotation. Introducing a *motB* allele that
245 prevents proton flux(40, 54) does not support flagellar signaling in the Δ*flgH* background (Fig 4A).
246 We conclude that proton translocation through MotB is required for flagellar perturbations to
247 stimulate holdfast production through the mechanical pathway. The finding that active proton
248 translocation is required for mechanical stimulation provides a possible explanation for the
249 disparate suppression patterns we observed in early and late flagellar assembly mutants. We
250 predicted that the mechanical pathway is inactive in early flagellar mutants because stator subunits
251 cannot engage with the motor when rotor assembly is incomplete. Indeed, Δ*fliF* was epistatic to
252 Δ*flgH* with respect to suppression by Δ*pleD* and Δ*motB* (Fig 4B). Adhesion in the Δ*fliF* Δ*flgH* mutant
253 was eliminated when *pleD* was deleted but remained unchanged when the Δ*motB* mutation was

254 introduced, supporting the model that inner membrane rotor assembly is required for activation of
255 the mechanical pathway.
256
257 **Discussion:**
258 Many bacteria alter their behavior upon contact with exogenous surfaces, and flagellar motility is a
259 key regulatory determinant of these responses(38, 55–58). However, efforts to dissect contact-
260 dependent signaling pathways have been confounded by contributions from multiple
261 mechanosensors(57, 59), a reliance on non-canonical signaling machinery(9, 40) and the
262 prevalence of transcription-independent responses(7, 60). In this study, we leveraged the hyper-
263 adhesive phenotype induced upon mutation of flagellar assembly genes to dissect the genetic basis
264 for adhesion control by the flagellum in *C. crescentus*. We used a high-throughput phenotyping
265 approach to identify mutations that stimulate adhesion and to classify a large group of genes called
266 *flagellar signaling suppressors* (*fss*) that contribute to increased holdfast production when flagellar
267 assembly is disrupted. The results have clarified important features of how the *C. crescentus*
268 flagellum regulates adhesion and provided a framework for disentangling signaling networks that
269 control bacterial behavior.
270 Two genes identified in the *fss* screen, *pleD* and *motB,* have been previously shown to link
271 flagellar function to adhesion, but conflicting models were proposed for how these genes regulate
272 holdfast production(34, 40). We found that *pleD* and *motB* participate in genetically distinct
273 pathways for activating adhesion. *pleD* and its downstream effector *shkA* contribute to increased
274 holdfast production when any stage of flagellar assembly is disrupted. *motB,* the gene for its
275 associated diguanylate cyclase, *dgcB*, and two previously uncharacterized motility genes contribute
276 to adhesion specifically in late flagellar mutants that retain the ability to assemble inner membrane

277 rotors. We conclude that a mechanical pathway and a developmental pathway operate in parallel to
278 link flagellar function to holdfast production.

279 Strains harboring deletions (Δ*motB,* Δ*fssA,* or Δ*fssB*) or mutant alleles (*motB*^{D33N}) that disrupt
280 motility without affecting filament assembly cannot support activation of the mechanical pathway
281 (Figs 2A, 3A and 4A). Additionally, early flagellar assembly mutants display epistatic effects on late
282 assembly mutants by eliminating *motB*'s involvement in stimulating adhesion (Fig 4B). These
283 results suggest that blocking inner membrane rotor (MS- and C-ring) assembly subverts the
284 mechanical pathway by preventing stator engagement and help to explain the range of behavioral
285 effects often observed in flagellar assembly mutants(5, 40, 61). We conclude that intact motors
286 capable of generating torque are required for mechanical activation of the *C. cresecentus* flagellum.
287 Increased load on rotating filaments leads to the recruitment of additional stators to the motor in
288 enteric bacteria(62, 63), and a similar resistance sensing mechanism likely supports tactile sensing
289 in *C. crescentus*. Mutants in mechanical pathway genes such as *fssA* and *fssB* should prove useful in
290 describing the structural basis for how such changes in load are sensed by the flagellar motor.

291 Key features of the mechanical pathway mirror the tactile sensing event described by Hug
292 and colleagues(40), but certain conclusions must be reevaluated in light of our results. Both early
293 and late flagellar mutants display increased holdfast production in liquid medium (Fig 2C), arguing
294 against a hyper-sensitive surface response in mutants lacking outer parts of the flagellum. Instead,
295 tactile sensing pathways appear to be activated ectopically in late flagellar mutants (Fig 2).
296 Preventing stators from productively engaging with the rotor, either by disrupting stator-associated
297 proteins or by mutating early flagellar genes that code for rotor components, blocks mechanical
298 signaling in late assembly mutants (Fig 4B). This explains the perplexing epistasis of inner parts of
299 the flagellum over outer parts(64) and supports established models for tactile sensing through
300 increased load on the filament(55) rather than the motor acting as tetherless sensor(40). More

301 broadly, the distinct phenotypes identified here for stator, rotor and hook-basal body mutants
302 support an emerging pattern seen in other organisms and likely represent a conserved feature of
303 bacterial flagella(65, 66).

304 The identification of a second, developmental pathway downstream of the flagellum is
305 consistent with previous studies showing that late flagellar assembly mutants display contact-
306 independent increases in holdfast production(33, 34). In fact, disrupting flagellar assembly at any
307 stage stimulates adhesion (Fig 2A), and our analysis of this process highlights an overlooked role
308 for the flagellum in controlling the *C. crescentus* developmental program. We explicitly
309 characterized *pleD* and *shkA*, but other developmental regulators identified in the *fss* screen (*shpA*,
310 *tacA*(46), *spmX*(67), *spmY*(68), *zitP, cpaM*(69), *sciP*(70), *rpoN*(71)) likely also act downstream of
311 both early and late flagellar mutants to stimulate adhesion. Most of these genes themselves
312 influence flagellar assembly. For instance, *pleD* promotes flagellar disassembly by stimulating
313 proteolytic turnover of the MS-ring protein FliF(72), but our results indicate that PleD is also
314 stimulated through phosphorylation at D53 when flagellar assembly is disrupted (Fig 4A). Thus, cell
315 cycle regulators that control the timing of flagellar assembly also act downstream of the flagellum
316 in regulating holdfast production. This duality raises the intriguing possibility that specific
317 environmental cues activate flagellar disassembly as part of a positive feedback loop that reinforces
318 the commitment to differentiate into a stalked cell.

319 The developmental and mechanical pathways we identified each require a distinct
320 diguanylate cyclase, supporting a model in which flagellar signaling converges to stimulate
321 adhesion by modulating c-di-GMP levels (Fig 4C). Signaling through the mechanical pathway
322 requires stator subunits that can productively engage with the rotor, and we propose that increased
323 load on the flagellar filament induces conformational changes in the motor that activate the stator-
324 associated diguanylate cyclase DgcB. This mechanism differs from contact-dependent activation of

325 c-di-GMP synthesis by SadC in *Pseudomonas aeruginosa*, which requires disengagement of the
326 MotCD stator(73). *P. aeruginosa* uses a MotAB stator system for swimming in liquid and a second,
327 MotCD stator for swarming on surfaces(74). Thus, the signaling competency of engaged stators in
328 *C. crescentus* could be an intrinsic feature of single-stator systems. Separately, c-di-GMP synthesis
329 by PleD is part of a multi-tiered system controlling the master cell-cycle regulator CtrA in *C.*
330 *crescentus*(48, 75), and our results suggest that the status of flagellar assembly feeds into this
331 developmental program by regulating PleD phosphorylation (Fig 4A). Whether the flagellum
332 controls PleD phosphorylation through the DivJ-PleC kinase-phosphatase pair(52) or through a
333 separate phosphorelay will require additional dissection of how *fss* genes link flagellar assembly to
334 cell cycle progression.

335 Using an unbiased screen to identify flagellar signaling genes has allowed us to propose a
336 unified model for the mechanism by which the flagellum regulates holdfast production in *C.*
337 *crescentus*. Intact flagellar motors respond to assembly defects in their associated filaments (Figs
338 2A and 4B), but perturbing the flagellum also influences the timing of holdfast production by
339 altering cell cycle signaling (34)(Figs 2A and 4A). Candidate approaches specifically targeting
340 developmental or tactile sensing phenomena have not accounted for presence of multiple pathways
341 downstream of the flagellum. Though two pathways can be distinguished genetically in flagellar
342 mutants, overlap between developmental, mechanical and other signaling pathways during actual
343 surface encounters has likely confounded interpretations of how the flagellum regulates holdfast
344 production. More broadly, our results underscore how bacterial behavior is not controlled by single,
345 linear signaling pathways. Flagellar cues represent only a subset of the stimuli known to influence
346 adhesion. Nutrient availability, redox homeostasis, chemotaxis and T4P dynamics all influence
347 whether *C. crescentus* produces a holdfast. Applying classical genetic principles in combination with

348 unbiased phenotyping approaches will continue to illuminate how the flagellar motility and other
349 behavioral process are integrated into broader developmental networks.
350
351 **Materials and Methods:**
352 *Bacterial growth and genetic manipulation*
353 Strains and plasmids used in the study are listed in Tables S4 and S5. Standard polymerase chain
354 reaction (PCR) and Gibson assembly(76) methods were used for developing plasmid constructs.
355 Strains, plasmids, primer sequences and details of construction are available upon request. *E. coli*
356 cultures were grown in LB medium at 37°C supplemented with 1.5% (w/v) agar and 50 μg/mL
357 kanamycin when necessary. Unless otherwise noted, *C. crescentus* cultures were grown at 30°C in
358 PYE medium supplemented with 1.5% (w/v) agar, 3% (w/v) sucrose and 25 μg/mL kanamycin
359 when necessary or in M2 defined medium supplemented with 0.15% (w/v) xylose (77). Plasmids
360 were introduced into *C. crescentus* by electroporation. Unmarked deletions were constructed using
361 *sacB*-based counterselection in sucrose.
362
363 *Genetic complementation of mutants*
364 Mutants were complemented by genomic integration of the appropriate gene as a single copy at a
365 neutral site (*xylX*) and under the gene's native promoter. Specifically, predicted open reading frames
366 were fused to their predicted promoter sequences and inserted into the NdeI/SacI site of pMT585
367 (pXGFPC-2)(78). Each promoter-gene cassette was inserted in reverse orientation to allow for
368 transcription in the opposite direction relative to the *xylX* promoter upstream of the cloning site.
369 Surface attachment and motility assays used to evaluate complementation are described below
370 (Figs S1 and S2).
371

372 *Tn-Himar mutant library construction and mapping*

373 Construction and mapping of the two barcoded transposon libraries was performed based on the
374 procedure developed by Wetmore et al. as described previously(33, 79). Cells from 25 mL cultures
375 of the APA_752 barcoded transposon pool that had been grown to mid-log phase in LB
376 supplemented with kanamycin and 300 μM diaminopimelic acid (DAP) and 25mL of either the *C.*
377 *crescentus* CB15 wild-type or Δ*flgH* strain that had been grown to mid-log phase in PYE were
378 collected by centrifugation, washed twice with PYE containing 300 μM DAP, mixed and spotted
379 together on a PYE agar plate containing 300 μM DAP. After incubating the plate overnight at room
380 temperature, the cells were scraped from the plate, resuspended in PYE medium, spread onto 20,
381 150mm PYE agar plates containing kanamycin and incubated at 30°C for three days. Colonies from
382 each plate were scraped into PYE medium and used to inoculate a 25mL PYE culture containing 5
383 μg/mL kanamycin. The culture was grown for three doublings, glycerol was added to 20%, and 1
384 mL aliquots were frozen at -80°C.

385 Library mapping was performed as described (79). Briefly, genomic DNA was isolated from
386 three 1mL aliquots of each library. The DNA was sheared and ~300bp fragments were selected
387 before end repair. A Y-adapter (Mod2_TS_Univ, Mod2_TruSeq) was ligated and used as a template
388 for transposon junction amplification with the primers Nspacer_BarSeq_pHIMAR and either
389 P7_mod_TS_index1 or P7_mod_TS_index2. 150-bp single end reads were collected on an Illumina
390 HiSeq 2500 in rapid run mode, and the genomic insertion positions were mapped and correlated to
391 a unique barcode using BLAT(80) and MapTnSeq.pl to generate a mapping file with
392 DesignRandomPool.pl. All code is available at https://bitbucket.org/berkeleylab/feba/. Features of
393 the barcoded transposon libraries can be found in Table S6.

394

395 *Adhesion profiling of barcoded Tn-Himar mutant libraries*

396 Adhesion profiling was performed as in Hershey et al. (33) with slight modifications. Cells from 1mL
397 aliquots of each barcoded transposon library were collected by centrifugation, resuspended in 1mL
398 of M2X medium, and 300 µL was inoculated into a well of a 12-well microtiter plate containing
399 1.5mL M2X medium with 6-8 ~1 x 1 cm layers of cheesecloth. Microtiter plates containing selections
400 were grown for 24hr at 30°C with shaking at 155rpm after which 150µL of the culture was passaged
401 by inoculating into a well with 1.65mL fresh M2X containing cheesecloth. Cells from an additional
402 500µL of depleted medium were harvested by centrifugation and stored at -20°C for BarSeq
403 analysis. Each passaging experiment was performed in triplicate, and passaging was performed
404 sequentially for a total of five rounds of selection. Identical cultures grown in a plate without
405 cheesecloth were used as a nonselective reference condition.

406 Cell pellets were used as PCR templates to amplify the barcodes in each sample using indexed
407 primers(79). Amplified products were purified and pooled for multiplexed sequencing. 50bp single
408 end reads were collected on an Illumina HiSeq4000. MultiCodes.pl, combineBarSeq.pl and FEBA.R
409 were used to determine fitness by comparing the $\log_2$ ratios of barcode counts in each sample over
410 the counts from a nonselective growth in M2X without cheesecloth. To evaluate mutant phenotypes
411 in each screen, the replicates were used to calculate a mean fitness score for each gene after each
412 passage. Mean fitness was summed across passages for each gene and ranked by either the lowest
413 (WT background) or highest (Δ*flgH* background) summed fitness score.

414

415 *Surface attachment measurement by crystal violet (CV) staining*

416 Overnight *C. crescentus* cultures grown in PYE were diluted to an OD_{660} of 0.5 with PYE, and 1.5 µL
417 from each diluted starter culture was inoculated into the wells of a 48-well microtiter plate
418 containing 450 µL M2X medium. The number of replicates for each experiment ranged from 5-8 and
419 is indicated in the relevant figure legend. Plates were grown at 30°C with shaking at 155rpm for 17

420 hours after which the cultures were discarded, and the wells were washed thoroughly under a
421 stream of tap water. Attached cells were stained by adding 500 μL of an aqueous solution containing
422 0.01% (w/v) crystal violet to each well and shaking the plates for 5 min. Excess dye was discarded,
423 the wells were again washed under a stream of tap water and the remaining dye was dissolved by
424 adding 500 μL of ethanol to each well. Staining was quantified by reading absorbance at 575nm
425 using a Tecan Spark microplate reader. Each reading was corrected by subtracting the absorbance
426 value for an uninoculated medium blank, the mean of the biological replicates for each strain was
427 calculated and normalized to the mean value measured for the wild type background. The collection
428 of strains shown in each figure was assayed together on at least four independent days and a
429 representative dataset is shown.
430
431 *Holdfast staining with fluorescent wheat germ agglutinin (fWGA)*
432 2mL of M2X medium was inoculated to achieve a starting OD_{660} of 0.001 using saturated starter
433 cultures grown in PYE. After growing to an OD_{660} of 0.07-0.1, 400 μL of each culture was added to a
434 fresh 1.5mL ependorf tube containing 1 μL of a 2mg/mL solution of WGA conjugated with Alexa594.
435 After a 5min incubation at room temperature in the dark, cells were harvested at 6k x g, washed
436 with distilled water, and resuspended in the residual liquid after centrifugation. 1 μL was spotted
437 onto a glass slide and a cover slip was placed on top. Imaging was performed with a Leica DM5000
438 microscope equipped with an HCX PL APO63X/1.4-numerical-aperture Ph3 objective. A red
439 fluorescent protein filter (Chroma set 41043) was used to visualize WGA foci. Cells with a holdfast
440 were counted manually on five separate days. A minimum of 95 cells were counted for each
441 biological replicate.
442
443 *Soft-agar motility assay*

444 Overnight cultures grown in PYE were diluted to OD_{660} = 0.5, and 1.5 μL was pipetted into a PYE
445 plate containing 0.3% agar. Plates were sealed with parafilm, incubated for 72 hours at 30°C and
446 photographed.
447
448 *Flagellar filament staining*
449 2mL of PYE medium was inoculated to a starting OD_{660} = 0.05 using saturated overnight starter
450 cultures and grown at 30°C to mid-log phase (OD_{660} = 0.3 – 0.4). 500 μL of each culture was mixed
451 with 0.5 μL of a 2mg/mL solution of Alexa488-maleimide in DMSO and incubated for 10min in the
452 dark. Cells were harvested by centrifuging at 6k x g for 1.5 min, washed with 500 μL PYE, re-
453 centrifuged and suspended in 500 μL PYE. 1 μL of the stained cell suspension was spotted on a pad
454 of PYE solidified with 1% agarose. Imaging was performed as above but with the use of green
455 fluorescent protein filter (Chroma set 41017) for flagellin visualization. Note that Alexa-488
456 maleimide cross-reacts with the holdfast.
457
458 *Microscopic analysis of swimming behavior*
459 2mL of PYE was inoculated to OD_{660} = 0.1 with saturated overnight starters and grown at 30°C to
460 OD_{660} = 0.4 – 0.5. A 2.69% (w/v) solution of 2.0 μm polystyrene spacer beads (Polysciences) was
461 diluted 1000-fold in 1mL PYE. Equal volumes of liquid culture and diluted spacer beads were mixed
462 and spotted on a slide. Dark field images were collected at 100ms intervals for 30s using a Leica 40X
463 PH2 objective. Maximum projections from each time series are presented.
464
465 *β-galactosidase assay*
466 Strains carrying a P_{hfiA}-*lacZ* transcriptional reporter (35) were inoculated from colonies on PYE-
467 agar plates into 2 ml M2X medium and grown shaking at 200 RPM overnight at 30°C. Overnight

468 cultures were diluted in 2 ml of fresh M2X to an OD_{660} of 0.05 and grown for approximately 6 hours
469 to early exponential phase. These cultures were then diluted again into 2 ml fresh M2X to an OD_{660} of
470 0.001 and grown for 17 hours to a final OD660nm of 0.1. β -galactosidase activity was then was
471 measured colorimetrically as previously described(35). Briefly, 0.15 ml of cells were permeabilized
472 by vortexing with 50 ul of chloroform and 50 ul of PYE broth as an emulsifier. 600 ul of Z-buffer (60
473 mM Na_2HPO_4, 40 mM NaH_2PO_4, 10 mM KCl, 1 mM $MgSO_4$) was added, followed by 200 ul ONPG in
474 0.1 M KPO_4. After 5 minutes at room temperature, reactions were quenched with 1 ml of 1 M Na_2CO_3
475 and absorbance at 420nm was used to calculate β -galactosidase activity.
476
477 *Data availability*
478 Sequence data have been deposited in the NCBI Sequence Read Archive (SRA) with the following
479 project accessions. For wild-type *C. crescentus,* PRJNA640825 contains the sequence data used to
480 map the barcoded TnHimar library, and PRJNA640525 contains barcoded amplicon sequences
481 collected after passaging in cheesecloth. For the Δ*flgH* mutant, PRJNA640725 contains the
482 sequencing data used to map the barcoded TnHimar library, and PRJNA641033 contains barcoded
483 amplicon sequences collected after passaging in cheesecloth.
484
485 **Acknowledgements**
486 We thank members of the Crosson laboratory, Howard Shuman and Phoebe Rice for helpful
487 discussions and insight. This work was supported by NIH grant R01GM087353 to S.C. D.M.H. is
488 supported by the Helen Hay Whitney Foundation.
489
490 **References**
491 1. Zobell CE. 1943. The Effect of Solid Surfaces upon Bacterial Activity. J Bacteriol 46:39–56.

492 2. Donlan RM. 2002. Biofilms: microbial life on surfaces. Emerg Infect Dis 8:881–890.

493 3. Chavez-Dozal A, Gorman C, Erken M, Steinberg PD, McDougald D, Nishiguchi MK. 2013.
494 Predation Response of *Vibrio fischeri* Biofilms to Bacterivorus Protists. Appl Environ
495 Microbiol 79:553–558.

496 4. Berne C, Ellison CK, Ducret A, Brun YV. 2018. Bacterial adhesion at the single-cell level. Nat Rev
497 Microbiol 16:616–627.

498 5. McCarter L, Hilmen M, Silverman M. 1988. Flagellar dynamometer controls swarmer cell
499 differentiation of *V. parahaemolyticus*. Cell 54:345–351.

500 6. Watnick PI, Kolter R. 1999. Steps in the development of a *Vibrio cholerae* El Tor biofilm. Mol
501 Microbiol 34:586–595.

502 7. Levi A, Jenal U. 2006. Holdfast Formation in Motile Swarmer Cells Optimizes Surface
503 Attachment during *Caulobacter crescentus* Development. J Bacteriol 188:5315–5318.

504 8. Mueller RS, McDougald D, Cusumano D, Sodhi N, Kjelleberg S, Azam F, Bartlett DH. 2007. *Vibrio*
505 *cholerae* Strains Possess Multiple Strategies for Abiotic and Biotic Surface Colonization. J
506 Bacteriol 189:5348–5360.

507 9. Petrova OE, Sauer K. 2011. SagS Contributes to the Motile-Sessile Switch and Acts in Concert
508 with BfiSR To Enable *Pseudomonas aeruginosa* Biofilm Formation. J Bacteriol 193:6614–
509 6628.

510 10. Collier J. 2016. Cell cycle control in Alphaproteobacteria. Curr Opin Microbiol 30:107–113.

511 11. Haiko J, Westerlund-Wikström B. 2013. The Role of the Bacterial Flagellum in Adhesion and
512 Virulence. Biology 2:1242–1267.

513 12. Belas R. 2014. Biofilms, flagella, and mechanosensing of surfaces by bacteria. Trends Microbiol
514 22:517–527.

515 13. Aldridge P, Hughes KT. 2002. Regulation of flagellar assembly. Curr Opin Microbiol 5:160–165.

516 14. Ramakrishnan G, Zhao JL, Newton A. 1994. Multiple structural proteins are required for both
517 transcriptional activation and negative autoregulation of *Caulobacter crescentus* flagellar
518 genes. J Bacteriol 176:7587–7600.

519 15. Stephens C, Mohr C, Boyd C, Maddock J, Gober J, Shapiro L. 1997. Identification of the *fliI* and
520 *fliJ* components of the *Caulobacter flagellar* type III protein secretion system. J Bacteriol
521 179:5355–5365.

522 16. Ohta N, Chen L-S, Swanson E, Newton A. 1985. Transcriptional regulation of a periodically
523 controlled flagellar gene operon in *Caulobacter crescentus*. J Mol Biol 186:107–115.

524 17. Jenal U. 2000. Signal transduction mechanisms in *Caulobacter crescentus* development and cell
525 cycle control. FEMS Microbiol Rev 24:177–191.

526 18. Khan S, Dapice M, Reese TS. 1988. Effects of *mot* gene expression on the structure of the
527 flagellar motor. J Mol Biol 202:575–584.

528 19. Blair DF, Berg HC. 1990. The MotA protein of *E. coli* is a proton-conducting component of the
529 flagellar motor. Cell 60:439–449.

530 20. Henrichsen J. 1972. Bacterial surface translocation: a survey and a classification. Bacteriol Rev
531 36:478–503.

532 21. Schneider WR, Doetsch RN. 1974. Effect of Viscosity on Bacterial Motility. J Bacteriol 117:696–
533 701.

534 22. Berg HC, Tedesco PM. 1975. Transient response to chemotactic stimuli in *Escherichia coli*. Proc
535 Natl Acad Sci USA 72:3235–3239.

536 23. Wadhwa N, Phillips R, Berg HC. 2019. Torque-dependent remodeling of the bacterial flagellar
537 motor. Proc Natl Acad Sci USA 201904577.

538 24. Pratt LA, Kolter R. 1998. Genetic analysis of *Escherichia coli* biofilm formation: roles of flagella,
539 motility, chemotaxis and type I pili. Mol Microbiol 30:285–293.

540 25. O'Toole GA, Kolter R. 1998. Flagellar and twitching motility are necessary for *Pseudomonas*
541 *aeruginosa* biofilm development. Mol Microbiol 30:295–304.

542 26. Bodenmiller D, Toh E, Brun YV. 2004. Development of surface adhesion in *Caulobacter*
543 *crescentus*. J Bacteriol 186:1438–1447.

544 27. Lauga E. 2016. Bacterial Hydrodynamics. Annu Rev Fluid Mech 48:105–130.

545 28. Shapiro L, Agabian-Keshishian N, Bendis I. 1971. Bacterial differentiation. Science 173:884–
546 892.

547 29. Poindexter JS. 1964. Biological properties and classification of the *Caulobacter* group. Bacteriol
548 Rev 28:231–295.

549 30. Degnen ST, Newton A. 1972. Chromosome replication during development in *Caulobacter*
550 *crescentus*. J Mol Biol 64:671–680.

551 31. Schmidt JM, Stanier RY. 1966. THE DEVELOPMENT OF CELLULAR STALKS IN BACTERIA. J Cell
552 Biol 28:423–436.

553 32. Poindexter JS. 1981. The caulobacters: ubiquitous unusual bacteria. Microbiol Rev 45:123–
554 179.

555 33. Hershey DM, Fiebig A, Crosson S. 2019. A Genome-Wide Analysis of Adhesion in *Caulobacter*
556 *crescentus* Identifies New Regulatory and Biosynthetic Components for Holdfast Assembly.
557 mBio 10:a000414-18.

558 34. Berne C, Ellison CK, Agarwal R, Severin GB, Fiebig A, Morton III RI, Waters CM, Brun YV. 2018.
559 Feedback regulation of *Caulobacter crescentus* holdfast synthesis by flagellum assembly via
560 the holdfast inhibitor HfiA. Mol Microbiol 9:e1003744-20.

561 35. Fiebig A, Herrou J, Fumeaux C, Radhakrishnan SK, Viollier PH, Crosson S. 2014. A Cell Cycle and
562 Nutritional Checkpoint Controlling Bacterial Surface Adhesion. PLoS Genet 10:e1004101-14.

563 36. Purcell EB, Siegal-Gaskins D, Rawling DC, Fiebig A, Crosson S. 2007. A photosensory two-
564 component system regulates bacterial cell attachment. Proc Natl Acad Sci U S A 104:18241–
565 18246.

566 37. Reyes Ruiz LM, Fiebig A, Crosson S. 2019. Regulation of bacterial surface attachment by a
567 network of sensory transduction proteins. PLoS Genet 15:e1008022.

568 38. Li G, Brown PJB, Tang JX, Xu J, Quardokus EM, Fuqua C, Brun YV. 2011. Surface contact
569 stimulates the just-in-time deployment of bacterial adhesins. Mol Microbiol 83:41–51.

570 39. Ellison CK, Kan J, Dillard RS, Kysela DT, Ducret A, Berne C, Hampton CM, Ke Z, Wright ER, Biais
571 N, Dalia AB, Brun YV. 2017. Obstruction of pilus retraction stimulates bacterial surface
572 sensing. Science 358:535–538.

573 40. Hug I, Deshpande S, Sprecher KS, Pfohl T, Jenal U. 2017. Second messenger–mediated tactile
574 response by a bacterial rotary motor. Science 358:531–534.

575 41. Sangermani M, Hug I, Sauter N, Pfohl T, Jenal U. 2019. Tad Pili Play a Dynamic Role in
576 *Caulobacter crescentus* Surface Colonization. mBio 10:740–18.

577 42. Dingwall A, Gober JW, Shapiro L. 1990. Identification of a *Caulobacter* basal body structural
578 gene and a cis-acting site required for activation of transcription. J Bacteriol 172:6066–6076.

579 43. Paul R, Weiser S, Amiot NC, Chan C, Schirmer T, Giese B, Jenal U. 2004. Cell cycle-dependent
580 dynamic localization of a bacterial response regulator with a novel di-guanylate cyclase
581 output domain. Genes Dev 18:715–727.

582 44. Leclerc G, Wang SP, Ely B. 1998. A new class of *Caulobacter crescentus* flagellar genes. J
583 Bacteriol 180:5010–5019.

584 45. Ellison CK, Rusch DB, Brun YV. 2019. Flagellar Mutants Have Reduced Pilus Synthesis in
585 *Caulobacter crescentus*. J Bacteriol 201:e00031-19.

586 46. Biondi EG, Skerker JM, Arif M, Prasol MS, Perchuk BS, Laub MT. 2006. A phosphorelay system
587 controls stalk biogenesis during cell cycle progression in *Caulobacter crescentus*. Mol
588 Microbiol 59:386–401.

589 47. Wolfe AJ, Visick KL. 2008. Get the Message Out: Cyclic-Di-GMP Regulates Multiple Levels of
590 Flagellum-Based Motility. J Bacteriol 190:463–475.

591 48. Kaczmarczyk A, Hempel AM, Arx C, Böhm R, Dubey BN, Nesper J, Schirmer T, Hiller S, Jenal U.
592 2020. Precise timing of transcription by c-di-GMP coordinates cell cycle and morphogenesis
593 in Caulobacter. Nature Communications 1–16.

594 49. Duerig A, Abel S, Folcher M, Nicollier M, Schwede T, Amiot N, Giese B, Jenal U. 2009. Second
595 messenger-mediated spatiotemporal control of protein degradation regulates bacterial cell
596 cycle progression. Genes Dev 23:93–104.

597 50. Lori C, Ozaki S, Steiner S, Böhm R, Abel S, Dubey BN, Schirmer T, Hiller S, Jenal U. 2015. Cyclic
598 di-GMP acts as a cell cycle oscillator to drive chromosome replication. Nature 523:236–239.

599 51. Sprecher KS, Hug I, Nesper J, Potthoff E, Mahi M-A, Sangermani M, Kaever V, Schwede T,
600 Vorholt J, Jenal U. 2017. Cohesive Properties of the *Caulobacter crescentus* Holdfast Adhesin
601 Are Regulated by a Novel c-di-GMP Effector Protein. mBio 8:e00294-17–15.

602 52. Aldridge P, Paul R, Goymer P, Rainey P, Jenal U. 2003. Role of the GGDEF regulator PleD in
603 polar development of *Caulobacter crescentus*. Mol Microbiol 47:1695–1708.

604 53. Hecht GB, Newton A. 1995. Identification of a novel response regulator required for the
605 swarmer-to-stalked-cell transition in *Caulobacter crescentus*. J Bacteriol 177:6223–6229.

606 54. Zhou J, Sharp LL, Tang HL, Lloyd SA, Billings S, Braun TF, Blair DF. 1998. Function of
607 Protonatable Residues in the Flagellar Motor of *Escherichia coli*: a Critical Role for Asp 32 of
608 MotB. J Bacteriol 180:2729–2735.

609 55. Alberti L, Harshey RM. 1990. Differentiation of *Serratia marcescens* 274 into swimmer and
610 swarmer cells. J Bacteriol 172:4322–4328.

611 56. Kawagishi I, Imagawa M, Imae Y, McCarter L, Homma M. 1996. The sodium-driven polar
612 flagellar motor of marine *Vibrio* as the mechanosensor that regulates lateral flagellar
613 expression. Mol Microbiol 20:693–699.

614 57. Laventie B-J, Sangermani M, Estermann F, Manfredi P, Planes R, Hug I, Jaeger T, Meunier E,
615 Broz P, Jenal U. 2019. A Surface-Induced Asymmetric Program Promotes Tissue Colonization
616 by *Pseudomonas aeruginosa*. Cell Host Microbe 25:140-152.e6.

617 58. Laganenka L, López ME, Colin R, Sourjik V. 2020. Flagellum-Mediated Mechanosensing and
618 RflP Control Motility State of Pathogenic *Escherichia coli*. mBio 11:e02269-19.

619 59. Güvener ZT, Harwood CS. 2007. Subcellular location characteristics of the *Pseudomonas*
620 *aeruginosa* GGDEF protein, WspR, indicate that it produces cyclic-di-GMP in response to
621 growth on surfaces. Mol Microbiol 66:1459–73.

622 60. Luo Y, Zhao K, Baker AE, Kuchma SL, Coggan KA, Wolfgang MC, Wong GCL, O'Toole GA. 2015. A
623 Hierarchical Cascade of Second Messengers Regulates *Pseudomonas aeruginosa* Surface
624 Behaviors. mBio 6:73–11.

625 61. Belas R, Suvanasuthi R. 2005. The ability of *Proteus mirabilis* to sense surfaces and regulate
626 virulence gene expression involves FliL, a flagellar basal body protein. J Bacteriol 187:6789–
627 6803.

628 62. Tipping MJ, Delalez NJ, Lim R, Berry RM, Armitage JP. 2013. Load-dependent assembly of the
629 bacterial flagellar motor. mBio 4:1–6.

630 63. Partridge JD, Nieto V, Harshey RM. 2015. A New Player at the Flagellar Motor: FliL Controls
631 both Motor Output and Bias. mBio 6:77–11.

632 64. Hughes KT, Berg HC. 2017. The bacterium has landed. Science 358:446–447.

633 65. Wu DC, Zamorano-Sánchez D, Pagliai FA, Park JH, Floyd KA, Lee CK, Kitts G, Rose CB, Bilotta
634 EM, Wong GCL, Yildiz FH. 2020. Reciprocal c-di-GMP signaling: Incomplete flagellum
635 biogenesis triggers c-di-GMP signaling pathways that promote biofilm formation. PLoS Genet
636 16:e1008703.

637 66. Harrison JJ, Almblad H, Irie Y, Wolter DJ, Eggleston HC, Randall TE, Kitzman JO, Stackhouse B,
638 Emerson JC, Mcnamara S, Larsen TJ, Shendure J, Hoffman LR, Wozniak DJ, Parsek MR. 2020.
639 Elevated exopolysaccharide levels in *Pseudomonas aeruginosa* flagellar mutants have
640 implications for biofilm growth and chronic infections. PLoS Genet 16:e1008848.

641 67. Radhakrishnan SK, Thanbichler M, Viollier PH. 2008. The dynamic interplay between a cell fate
642 determinant and a lysozyme homolog drives the asymmetric division cycle of *Caulobacter*
643 *crescentus*. Genes Dev 22:212–225.

644 68. Janakiraman B, Mignolet J, Narayanan S, Viollier PH, Radhakrishnan SK. 2016. In-phase
645 oscillation of global regulons is orchestrated by a pole-specific organizer. Proc Natl Acad Sci U
646 S A 113:12550–12555.

647 69. Mignolet J, Holden S, Bergé M, Panis G, Eroglu E, Théraulaz L, Manley S, Viollier PH. 2016.
648 Functional dichotomy and distinct nanoscale assemblies of a cell cycle-controlled bipolar
649 zinc-finger regulator. eLife 5:e20640-21.

650 70. Tan MH, Kozdon JB, Shen X, Shapiro L, McAdams HH. 2010. An essential transcription factor,
651 SciP, enhances robustness of *Caulobacter* cell cycle regulation. Proc Natl Acad Sci U S A
652 107:18985–18990.

653 71. Anderson DK, Ohta N, Wu J, Newton A. 1995. Regulation of the *Caulobacter crescentus rpoN*
654 gene and function of the purified σ54 in flagellar gene transcription. Mol Gen Genet 246:697–
655 706.

656 72. Aldridge P, Jenal U. 1999. Cell cycle-dependent degradation of a flagellar motor component
657 requires a novel-type response regulator. Mol Microbiol 32:379–391.

658 73. Baker AE, Webster SS, Diepold A, Kuchma SL, Bordeleau E, Armitage JP, O'Toole GA. 2019.
659 Flagellar Stators Stimulate c-di-GMP Production by *Pseudomonas aeruginosa*. J Bacteriol
660 201:263–13.

661 74. Toutain CM, Zegans ME, O'Toole GA. 2005. Evidence for Two Flagellar Stators and Their Role
662 in the Motility of *Pseudomonas aeruginosa*. J Bacteriol 187:771–777.

663 75. Quon KC, Marczynski GT, Shapiro L. 1996. Cell Cycle Control by an Essential Bacterial Two-
664 Component Signal Transduction Protein. Cell 84:83–93.

665 76. Gibson DG, Young L, Chuang R-Y, Venter JC, Hutchison CA, Smith HO. 2009. Enzymatic
666 assembly of DNA molecules up to several hundred kilobases. Nat Methods 6:343–345.

667 77. Ely B. 1991. Genetics of Caulobacter crescentus. Meth Enzymol 204:372–384.

668 78. Thanbichler M, Iniesta AA, Shapiro L. 2007. A comprehensive set of plasmids for vanillate- and
669 xylose-inducible gene expression in *Caulobacter crescentus*. Nucleic Acids Res 35:e137–e137.

670 79. Wetmore KM, Price MN, Waters RJ, Lamson JS, He J, Hoover CA, Blow MJ, Bristow J, Butland G,
671 Arkin AP, Deutschbauer A. 2015. Rapid Quantification of Mutant Fitness in Diverse Bacteria
672 by Sequencing Randomly Bar-Coded Transposons. mBio 6:e00306-15–15.

673 80. Kent WJ. 2002. BLAT—The BLAST-Like Alignment Tool. Genome Res 12:656–64.

674

675

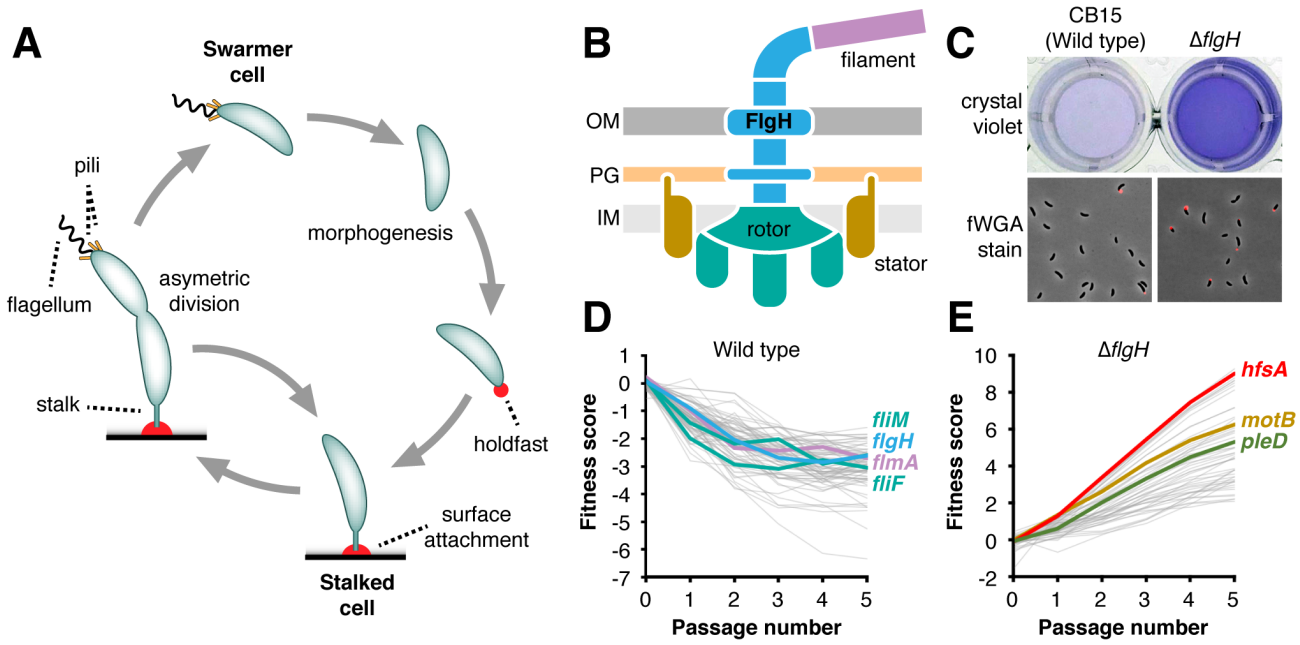

676

677 **Figure 1** *Identifying genes that link the flagellum to holdfast production*

678 A) The asymmetric division cycle of *C. crescentus*. Sessile stalked cells divide to release a newborn
679 swarmer cell that displays a flagellum and type IV pili. Quiescent swarmer cells undergo a
680 morphological transition to become replication competent stalked cells. Transitioning swarmer
681 cells can make an adhesin called the holdfast (red) that promotes surface attachment. B) Schematic
682 of flagellar architecture. A central hook-basal body (HBB) complex (blue) spanning the cell envelope
683 tethers a long extracellular filament (purple) to the surface of the cell. Multiple stator subunits
684 (gold) that surround the inner membrane embedded rotor (teal) use ion translocation to turn the
685 HBB and its associated filament. Outer membrane (OM), peptidoglycan (PG) and inner membrane
686 (IM) layers of the envelope are shown. C) The Δ*flgH* mutant shows increased surface colonization
687 (top), as measured by crystal violet (CV) staining, and a higher proportion of holdfast producing
688 cells relative to wild type (bottom). Holdfasts were stained with Alexa 594-wheat germ agglutinin
689 (fWGA). D) Hyper-adhesive mutants identified by adhesion profiling in defined medium. The 75
690 genes with the strongest hyper-adhesive profiles are plotted, and specific flagellar assembly genes

691 are highlighted. Colors correspond to the structural proteins depicted in panel B. The plotted genes
692 are listed in Table S1. E) The *flagellar signaling suppressor* (*fss*) genes identified by adhesion
693 profiling in the Δ*flgH* background. The 50 genes with the strongest contributions to adhesion in the
694 Δ*flgH* background are plotted. *hfsA*, a gene required for holdfast biosynthesis, is highlighted along
695 with two *fss* genes, *pleD* and *motB.* The plotted genes are listed in Table S2. For panels D and E, each
696 line represents the average fitness values for a single gene plotted as a function of time in the
697 sequential passaging experiment. Hyper-adhesive mutants are depleted more rapidly than neutral
698 mutants during selection in cheesecloth. Mutated genes (*fli*, *flg, flm,* etc.) that display increased
699 attachment to cheesecloth show steadily decreasing fitness scores as a function of passage number.
700 Mutants with reduced adhesion are enriched in broth when grown with cheesecloth. Mutated genes
701 that display decreased adhesion (*hfs* and *fss*) show steadily increasing fitness scores.
702

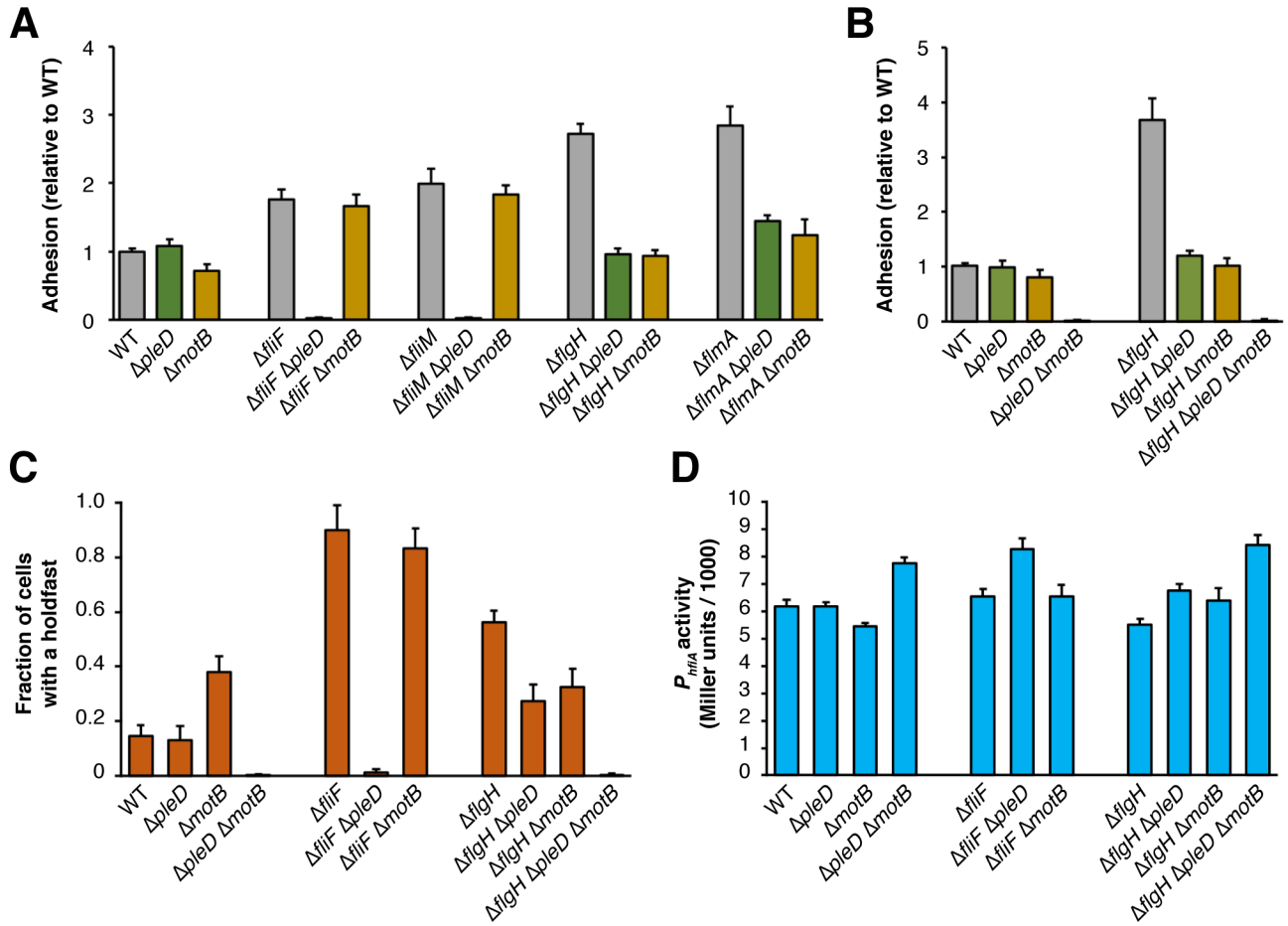

Figure 2 *Two distinct signaling pathways operate downstream of the flagellum to control adhesion* A) Crystal violet-based attachment assay showing suppression of the hyper-adhesive phenotypes by *pleD* and *motB* in early (Δ*fliF* and Δ*fliM*) and late (Δ*flgH* and Δ*flmA*) flagellar assembly mutants. Mean values from six biological replicates are shown with error bars representing the associated standard deviations. B) Crystal violet-based attachment assay showing the additive effects of Δ*motB* and Δ*pleD* on adhesion in the WT and Δ*flgH* backgrounds. Mean values from five biological replicates are shown with the associated standard deviations. C) Fraction of cells with a holdfast in flagellar mutant and suppressor backgrounds. Holdfasts were stained and counted from log phase cultures as described in Materials and Methods. D) *hfiA* transcription in flagellar mutant and suppressor backgrounds as measured by beta-galactosidase activity from a P_{hfiA}-*lacZ* reporter. Mean values from three biological replicates collected on two separate dates for a total of six replicates

715 are shown with the associated standard deviations. A statistical analysis of the CV staining, holdfast

716 count and LacZ activity measurements is reported in Table S3.

717

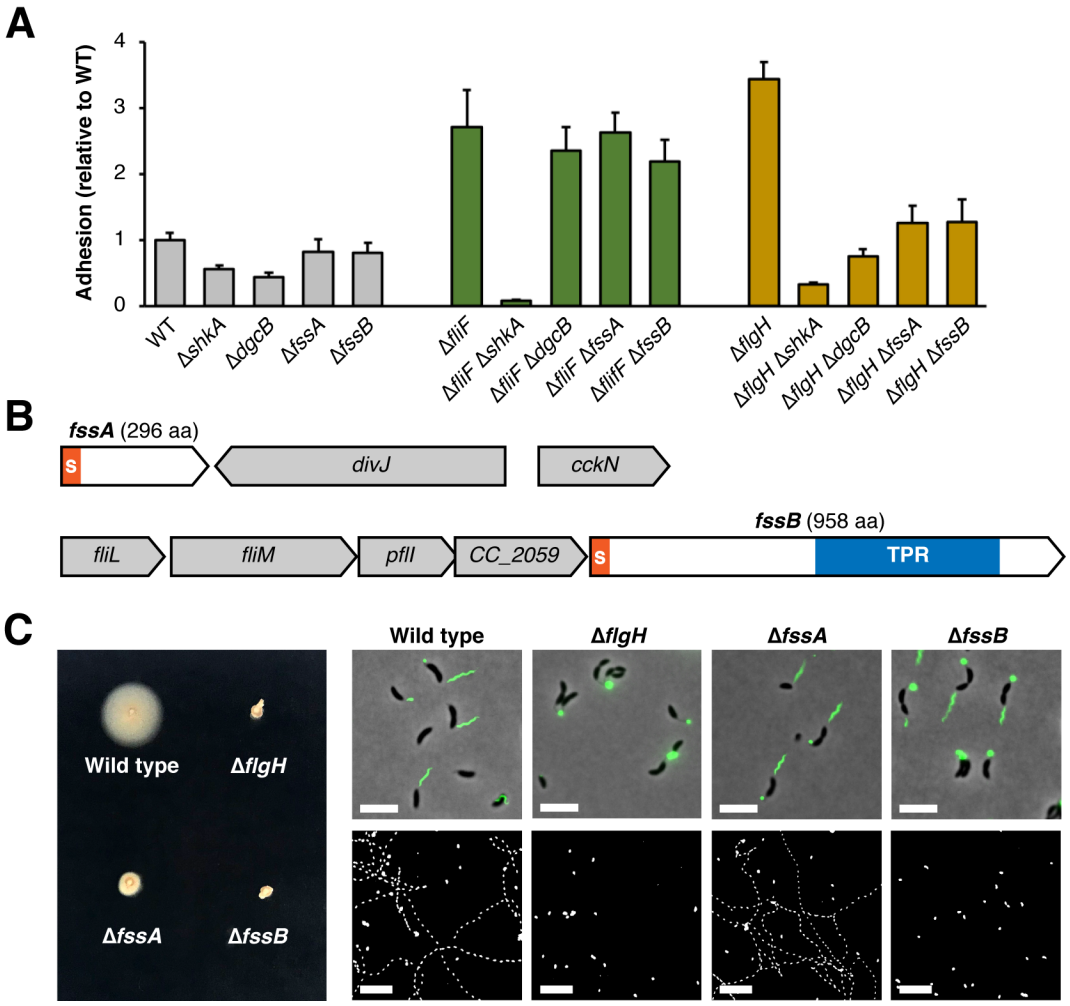

Figure 3 *Two novel motility genes contribute to activation of the mechanical pathway*

A) Crystal violet-based attachment assay showing suppression of early and late flagellar assembly mutants by individual *fss* genes. Mean values from six biological replicates are shown with error bars representing the associated standard deviations. B) Genomic context of the *fssA* and *fssB* genes. Orange S: secretion signal; blue bar: tetratricopeptide repeat region. C) Motility phenotypes of the Δ*fssA* and Δ*fssB* mutants. Left: soft-agar motility assay. Top right: flagellar filaments stained with Alexa488-maleimide after introduction of the $fljK^{T103C}$ allele into the indicated mutants. Note that the maleimide dye cross-reacts with holdfast. Scale bars represent 5μm. Bottom right: maximum projections from time-lapse microscopy. Cells appear in white, and tracks for motile cells appear as dotted lines. Scale bars represent 25μm.

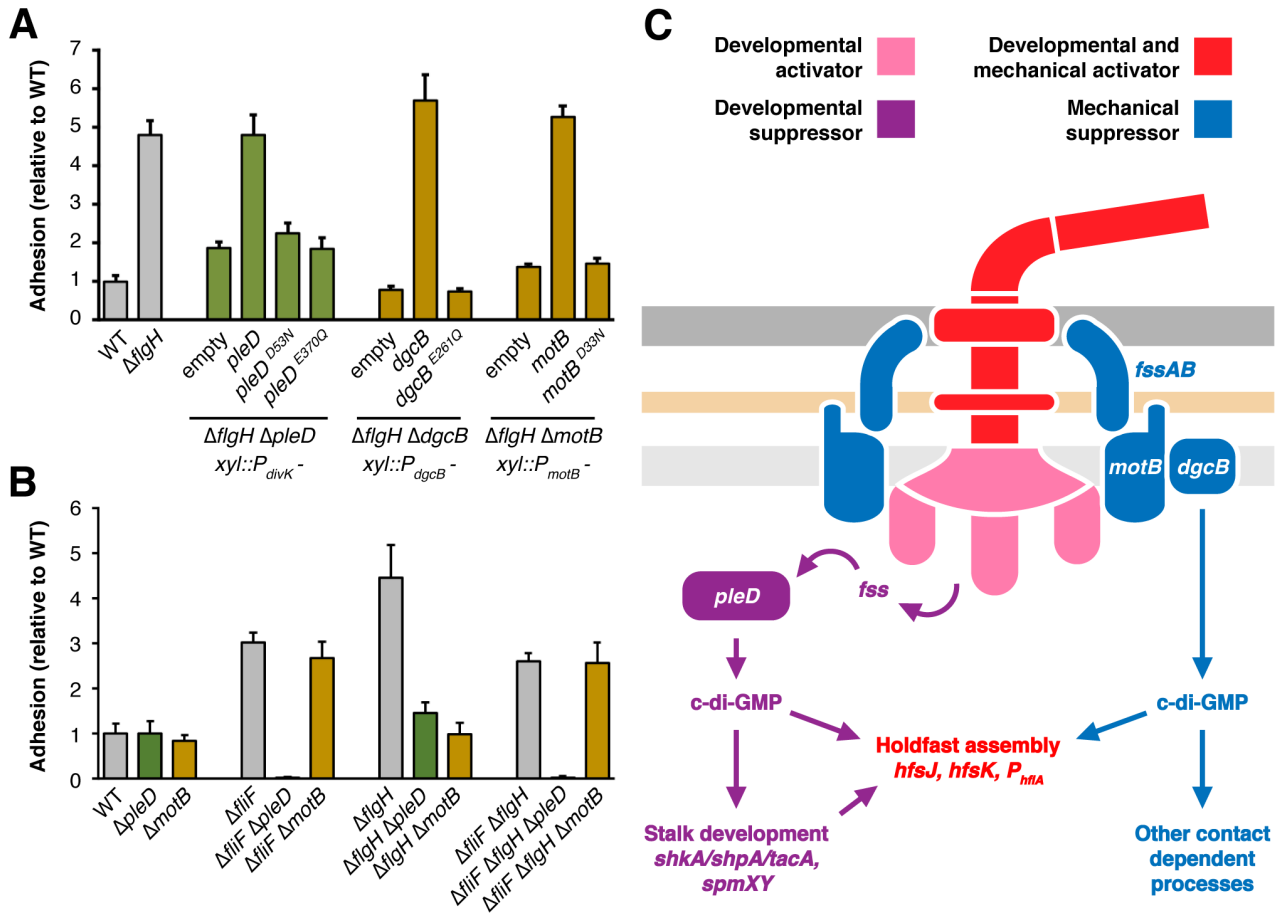

Figure 4 *Convergence of flagellar signaling on cyclic-di-GMP*

A) Crystal violet-based attachment assay showing that inactive alleles of *fss* genes in the developmental (*pleD*) and mechanical (*dgcB* and *motB*) pathways do not support flagellar signaling. Each allele is expressed from the gene's native promoter and integrated as a single copy at the *xylX* locus. The genotype and promoter for each strain are indicated below the solid line. Mean values from seven biological replicates are shown with error bars representing the associated standard deviations. B) Crystal violet-based attachment assay showing that early flagellar mutants are epistatic to late flagellar mutants for activation of the mechanical pathway. The Δ*fliF* Δ*flgH* strain phenocopies the Δ*fliF* strain and demonstrates that the effect of *motB* on adhesion requires early stages of flagellar assembly. Mean values from five biological replicates are shown with the associated standard deviations. C) Two signaling pathways operate downstream of the flagellum in

742 *C. crescentus.* Disrupting the assembly of the flagellum at any stage stimulates adhesion by activating
743 a developmental pathway that requires PleD phosphorylation. Separately, mechanical signals are
744 transmitted through the motor to activate DgcB. Both PleD and DgcB stimulate holdfast production
745 by modulating c-di-GMP levels in response to flagellar perturbation.
746
747

748 **Supplemental files**

749 *Table S1 – Mutated genes that produce a hyper-adhesive phenotype during adhesion profiling*

750 *Table S2 – Mutated genes that suppress hyper-adhesion in the Δ*flgH *background during adhesion*

751 *profiling*

752 *Table S3 – Statistical analysis of strain comparisons shown in Figure 2*

753 *Table S4 – Plasmids used in this study*

754 *Table S5 – Strains used in this study*

755 *Figure S1 – Genetic complementation of surface attachment and motility phenotypes for flagellar*

756 *assembly hierarchy mutants*

757 *Figure S2 -Genetic complementation of attachment and motility phenotypes of* fss *mutants*

758 *Table S6 – Features of the barcoded transposon libraries used in this study*

759